# A STUDY ON
# TOOL LIFE OF GRINDING WHEELS

By
JAGDISH PRASAD MEHTA



DEPARTMENT OF MECHANICAL ENGINEERING
INDIAN INSTITUTE OF TECHNOLOGY KANPUR
AUGUST 1974

# A STUDY ON TOOL LIFE OF GRINDING WHEELS

A Thesis Submitted
In Partial Fulfilment of the Requirements
for the Degree of
MASTER OF TECHNOLOGY

By
JAGDISH PRASAD MEHTA

to the

DEPARTMENT OF MECHANICAL ENGINEERING
INDIAN INSTITUTE OF TECHNOLOGY KANPUR
AUGUST 1974

TO

MY LOVING MA

CERTIFICATE

Certified that this work on " A STUDY ON TOOL LIFE OF GRINDING WHEELS " by Jagdish Prasad Mehta has been carried out under my supervision and that this work has not been submitted elsewhere for a degree.

Dr. G.K. Lal
Assistant Professor
Department of Mechanical Engineering
Indian Institute of Technology, Kanpur

ACKNOWLEDGEMENTS

I am deeply indebted to Dr. G.K. Lal for his invaluable counsel, encouragement, guidance and the confidence he has inspired in me to make this work possible in the present form.

I wish to express my sincere appreciation of the assistance I obtained from Mr. Joginder Singh, Senior Technical Assistant in the Department of Mechanical Engineering.

I remain grateful to my friends specially Lt. G.R. Bajaj and Mr. K. Mathur for many occasions of fruitful discussions with them.

I wish to thank Mr. D.P. Saini for typing the manuscript neatly.

J.P. Mehta.

CONTENTS

## NOMENCLATURE

| | |
|---|---|
| $a$ | = Number of active arms in the wheatstone bridge |
| $b$ | = Mean width of chip |
| $b_r$ | = Width of the ring(octagonal) |
| $b_w$ | = Width of the workpiece |
| $C$ | = Static constant of tool life equation |
| $c$ | = Number of cutting edges per unit area of wheel face |
| $D_e$ | = Equivalent diameter |
| $D_G$ | = Wheel diameter |
| $\delta(D_G)$ | = Reduction in wheel diameter |
| $D_w$ | = Work diameter |
| $d$ | = Depth of cut |
| $E$ | = Young's modulus of dynamometer ring material |
| $E_w$ | = Input voltage to wheatstone bridge |
| $F_n$ | = Normal force component |
| $F_t$ | = Tangential force component |
| $f_n$ | = Natural frequency of dynamometer ring |
| $G$ | = Grinding ratio |
| $G_f$ | = Gauge factor of strain gauge |
| $h_w$ | = Height of the workpiece |
| $K_{nn}, K_{nt}, K_{tn}, K_{tt}$ | are constants of calibration curve |
| $l$ | = Length of chip |
| $l_w$ | = Length of workpiece |
| $M$ | = Mass of the dynamometer ring |

| | |
|---|---|
| $N^*$ | = Tool life of grinding wheel in terms of number of up-strokes |
| $n$ | = Exponent of tool life equation |
| $R$ | = Resistance of strain gauge |
| $r$ | = Ratio of mean width to mean thickness of chip |
| $\Delta R$ | = Change in resistance of the strain gauge |
| $R_i$ | = Radius of inside surface of the octagonal ring |
| $R_n$ | = Deflection due to normal force |
| $R_t$ | = Deflection due to tangential force |
| $S$ | = Spring constant of the dynamometer ring |
| $T^*$ | = Tool life of grinding wheel in seconds |
| $t$ | = Maximum chip thickness |
| $t_r$ | = Minimum thickness of the octagonal ring |
| $V$ | = Wheel speed |
| $v$ | = Table speed |
| $V_R$ | = Material removal rate |
| $V_w$ | = Volume of material removed |
| $\epsilon_t$ | = Longitudinal tensile strain in the strain gauge |
| $\sigma_{max}$ | = Maximum stress induced in the octagonal ring |

## SYNOPSIS

Tool life of grinding wheels may be established from the consideration of grinding forces, wheel wear and surface finish. In the present work experimental study of horizontal surface grinding process has been carried out to establish force patterns using a two-component dynamometer which was fabricated for the purpose. From force plots tool life of grinding wheel has been evaluated and an attempt has been made to establish the possible existence of an empirical relationship for wheel life under various cutting conditions. The tool life has been found to be function of rate of material removal. No definite conclusion is, however, intended since the data available were limited.

Reduction in wheel diameter has been measured to find the volume of wheel wear from which economic considerations for the selection of grinding wheels has been investigated. Experiments also show that an optimum grinding ratio is obtained when various grinding wheels are used for a particular material. This should be an important consideration in the selection of grinding wheels.

CHAPTER-1

# INTRODUCTION AND LITERATURE REVIEW

## 1.1 General

In most metal cutting processes a tool of known geometry and orientation is used, but in grinding a large number of grains, acting as cutting points are randomly distributed across the surface of the wheel. High cutting speed (about 1800 m/min), small grain depth of cut (about 10 $\mu$ or less) and considerable side flow due to small lateral extent of an individual grain, are the three aspects in which grinding differs from single point cutting. The geometry of abrasive grains not only varies from grain to grain but it also changes continuously as the grinding is continued. Thus, in grinding, the ordinary variable of metal-cutting such as rake angles etc. which are so important in the theoretical study can not be measured directly, but instead only an average can be taken of all grains involved in the process.

The specific energy (energy required to remove a unit volume of material) in grinding has been found to be about 50 times that involved in turning (9). This has been explained in terms of the "size effect". It is a matter of common experience that the greater the degree of sub-division involved in dismantling a body, the greater is the energy expended.

In the grinding operation, the chip are very finely divided so that this form of material removal may be expected to require a high specific energy. It has been found (19) that when the maximum chip thickness is less than about 30 $\mu$in., the shear strength of the metal approaches its theoretical value. The attainment of this theoretical value of strength has been attributed to the grain depth of cut, being so small that the material is sheared between two atomic planes.

1.2 Effective Rake Angle of an Individual Grain:

In single point cutting it has been found (22) that the ratio of tangential to normal force is strongly dependent on the rake angle of the tool. This ratio decreases as the rake angle is reduced and for tools having large negative rake angles, the value of force ratio approximates 0.5. If this analogy with single point cutting is correct then the typical abrasive grain would, on the average, have a negative rake angle. In their work Becker and Merchant (17) compared the ratios of the tangential and normal forces obtained when grinding, with those found when turning, and suggested that the mean effective rake angle of a grinding grain should be nearly - 30°.

In an alternative treatment, Hahn (21,23) suggested that it is more realistic to consider the frictional rubbing forces on the clearance surface and neglect the cutting forces acting on the rake face. This concept led him to introduce his "rubbing grain" hypothesis, in which he emphasized the importance of a dull grit. He observed that tools having

a very small clearance angle ($\simeq 0.5°$) produced no chips at small depth of cut (less than 0.0004 in.). In this regime the force ratio is small due to the forces acting on the clearance face. In this manner Hahn explained the small force ratios observed when grinding. However, no change in force ratio is observed with decreasing depth of cut when using tools having large negative rake angles (26). Therefore, the existence of a small force ratio when grinding may be explained in terms of an average grain having a large negative rake angle.

1.3 Chip Thickness

Maximum chip thickness (t) is the most important geometrical quantity in any grinding operation. All chips are assumed to have the same size, and in order to be sure that all the metal to be removed is accounted for, the chips are assumed to be of constant width (Fig. 1.1 - a). Actually grinding chips will be shaped as in Fig. 1.1- b, where the mean cross-section is the same as in Fig. 1.1- c.

Assuming that the variation of chip thickness is triangular in shape, chip length is given by,

$$l = \sqrt{D_g d} \qquad \ldots \qquad \ldots \qquad \ldots \qquad (1.1)$$

where,

$l$ = Undeformed chip length

$D_g$ = Wheel diameter

$d$ = Wheel depth of cut.

Continuity consideration for metal removal rate gives (13)

$$t = \left[\frac{4r}{Vcr}\sqrt{d/De}\right]^{1/2} \quad \ldots \quad \ldots \quad \ldots \quad (1,2)$$

where,

t = Maximum chip thickness

v = Table speed

V = Wheel speed

c = Number of cutting edges per unit area of wheel face

$r = \frac{\text{Mean width of chip 'b'}}{\text{Mean thickness of chip t/2}}$

De = Equivalent diameter, depending upon the type of grinding operation.

$De = \frac{D_w D_g}{D_w + D_g}$ .... For external grinding

$= \frac{D_w D_g}{D_w - D_g}$ .... For internal grinding

$= D_g$ .... For surface grinding

where,

$D_w$ = Work piece diameter.

1.4 Grinding Action

In order to study grinding action Hahn (25) used controlled force plunge grinding, in which grinding wheel was pressed against the work piece with prescribed force instead of prescribed feed rate. The radial feed was proportional to the radial stock removal rate. He found that radial feed rate was small under light load and the work piece is ploughed by the

grains forming groove with small metal particals on the sides of the groove. As the load is increased the feed rate increases and beyond a certain load, rapid stock removal occurs, when conventional chips are produced. At very light load there is little or no stock removal and rubbing occurs.

Lal & Shaw (11) explained grinding action by using mounted grains to produce a single groove on a tapered specimen. They adopted increasing depth of cut by moving the work piece under the wheel. At the beginning of a cut the value of d was small resulting in the ploughing of material to the sides of the groove. At some point along the tapered workpiece the depth of cut approaches the critical value, which defines the chip formation. These results are shown in Fig. (1.4). The intermediate range is the unstable portion of the curve and shows the change from ploughing to cutting. They concluded that a curve similar to that shown in Fig. (1.4) will be obtained if the depth of cut are plotted along the chip length. Thus it implies that there is transition from rubbing to cutting during every cut.

## 1.5 Grinding Wheel Wear

### 1.5.1 Types of wheel wear

Grindability describe the relative ease of grinding and is comparable to machinability for single point tool cutting. Grindability is mathematically expressed by grinding ratio (volume of material removed by unit volume of wheel wear). Criterion for grinding wheel selection is normally based on the optimum grinding ratio.

The nature of grinding wheel wear has been the subject of numerous investigations in the past. The physical properties of abrasive wear have been discussed by Wagner (4), and by Goepfert and Williams (32) while others (17,20,33) have directed their investigations towards the solution of practical problems. The mechanism involved in the process have been studied more recently by several investigators (30, 31,33,34,39,40,42,44).

The wear of grinding wheel is both physical and chemical in nature. The relative significance of each of these types on the overall wear depends on the wheel-work material combination and grinding conditions.

Physical wear of wheel can be understood from the relationship of the physical properties of the abrasive on the wheel and the work material. Three types of physical wear have been observed. These are illustrated in Fig. (1.2).

Attritious wear occurs on the grain-workpiece contact surface (a) and it is generally accepted that plastic flow and chemical reaction (36,37) have significant effect on this phenomenon. This results in dulling of the abrasive grains and accounts for the glazed appearance of a grinding wheel. When this type of wear is predominant the grinding ratio is high.

Fracture wear, on the other hand, is due to the removal of abrasive particals from the wheel either by partial fracture of grains (b) or by fracturing of the bond post (c) as shown in Fig. 1.2. Fracture wear results in a low grinding ratio but maintains the cutting ability of the wheel by presenting sharp cutting edges without dressing. This phenomenon

is called the self-dressing, which leads to lower cutting forces and temperatures. The mechanics of fracture wear has been analysed by Yoshikawa(44) and Yoshikawa & Sata (39) using theories of nucleation and stochastic processes. Their relationship predict the wear rate in terms of the forces on an average grain, the grinding time, amount of bond in the wheel and average size of a fractured grain. A further experimental investigation of fracture wear has been recently carried out by Wilkin and Cook (34).

1.5.2 Typical wheel wear pattern

The sequence of events for flank wear development in single point cutting tool (Fig. 1.5) is initial breakdown (region I where the sharp cutting edge is quickly broken down and a finite wear land is established) then uniform wear rate (region II) and the final gradually increasing wear rate (region III). Curves relating the volume of grinding wheel wear to the volume of metal removed has been found (33) to be similar in nature to wear curve for a single point cutting tool. Typical grinding wheel wear curve is shown in Fig. 1.5, which shows three distinct regions:

Region I: A short period of nonlinear rapid wear - when the wheel first contacts the workpiece there is rapid breakdown of fine sharp points left from the dressing. Grinding ratio in this region is low.

Region II: Longer period of constant and slow wear rate - this is the normal operating portion of the wheel wear curve, which characterises good grinding conditions. For particular

operating conditions this region gives highest grinding ratio, which is taken as representative value of grinding ratio for those conditions.

Region III: A region of sharp increase in wear rate this results when either the wheel is overloaded and stable or excessive vibrations develop and wheel wear occurs due to fracture wear which dominate attritious wear. This region characterizes poor grinding conditions and results in low value of grinding ratio.

As grinding proceeds and the abrasive grains take repeated contacts with the workpiece, the sharp edges are worn away producing flat areas on the grain. Gradual increase in flat areas increases the force on the grain until it becomes sufficient to cause fracture of the grain or bond post holding the grain. When the large percentage of active grain reaches this conditions grinding approaches region III. If the bond posts are too strong or grain is not sufficiently friable then wheel face will appear glazed and redressing is required to restore the cutting ability of the grains. If, however, a wheel of proper grade in used, the nature and proportion of, attritious and fracture wear may be such that the wheel will tend to be self-dressing, resulting in extended region II, giving optimum grinding ratio.

1.6 Present Work

Economic aspect of grinding process have been discussed by some of the investigators (30,54,55). During the grinding wheel wear study Backer

& Merchant (17) and Grisbrook, Wollner and Harley (46) concluded that loss of wheel is mainly due to diamond dressing. Ital & Stetiu (30) studied wheel life (work-time between two successive dressings) of grinding wheel, and presented approximate relationship between wheel life and depth of cut. They mentioned in their work that the method they have adopted for establishing wheel life was somewhat crude. Force pattern during grinding was also established by some of the workers (45, 46) but no attempt was made by them to investigate grinding forces with the consideration of cost of grinding. They concluded that the force pattern during grinding is similar to the wheel wear curve.

It seems that force pattern may be important criteria to predict the tool life of grinding wheel. In the present work an attempt has been made to evaluate wheel life from the force pattern and co-relate it with table speed and depth of cut.

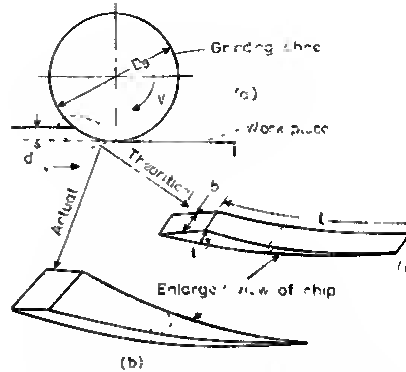


FIG 1 1 GRINDING GEOMETRY (a) SURFACE GRINDING OPERATION (b) ACTUAL SHAPE OF CHIP (c) THEORITICAL SHAPE OF CHIP

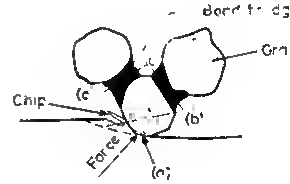


FIG 1 2 THREE TYPES OF GRINDING WHEEL WEAR
(a) ATTRITIOUS WEAR OF GRAIN
(b) MECHANICAL FRACTURE OF GRAIN
(c) FRACTURE OF BOND BRIDGES

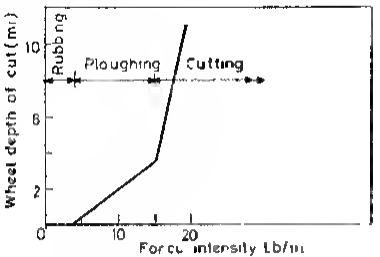


FIG 1 3 WHEEL DEPTH OF CUT VS FORCE INTENSITY (AFTER HAHN[25])

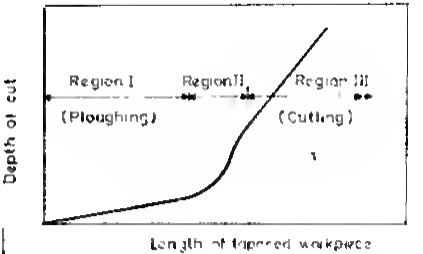


FIG 1 4 DEPTH OF CUT VS TAPERED WORK PIECE LENGTH (AFTER LALRSHAW[11])

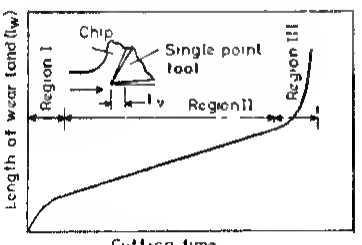


FIG 1 5 DEVELOPMENT OF FLANK WEAR WITH TIME

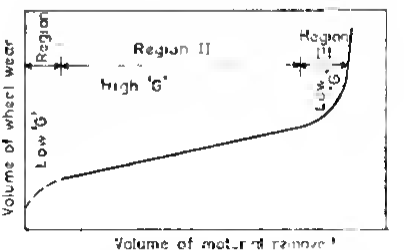


FIG 1 6 GRINDING WHEEL WEAR CURVE (AFTER KRABACHER[33])

## CHAPTER 2

## TWO-COMPONENT GRINDING DYNAMOMETER

### 2.1 General:

Grinding force is an important parameter in predicting the performance of a grinding wheel. Marshall and Shaw (47) were probably the first to measure grinding forces with the help of a specially designed two-component dynamometer. Since then more sophisticated devices have been built and tested.

### 2.2 Design Requirements:

Two main requirements of a dynamometer which oppose each other are sensitivity and stiffness. The sensitivity of a dynamometer should be such that determinations are accurate to within $\pm$ 1%. High stiffness of the dynamometer is also essential to avoid interference with the normal cutting operation of the wheel. In order that the recorded force is not influenced by any vibratory motion of the dynamometer its natural frequency must be about four times more than that of the exciting vibration (26).

Surface grinding dynamometer should measure two components of the grinding force ( that is, normal and tangential components) with minimum cross sensitivity. It should also be stable with respect to time temperature and humidity.

2.3 Force Measuring Devices:

In general force measurement involves the measurement of deflection with a suitable calibration between the force and the deflection it produces. Some devices for measuring small deflection are dial indicators, hydraulic pressure cells, pneumatic devices, piezoelectric crystals and electric resistance strain gauges.

With the development of high quality amplifying and recording equipment, bonded electric resistance strain gauges are perhaps most suitable for such measuring devices. They can be mounted directly to the dynamometer ring thus eliminating the need for a separate pickup device.

2.4 The Wheatstone Bridge.

Although actual resistance changes in a strain gauge are very small, they are readily measured by connecting the gauges in the form of a wheatstone bridge. The gauges are connected in such a way that there is an increase in resistance in opposite arms and decrease in the other two arms, which combine to increase the output voltage. Also equal changes in the resistance of adjacent arms causes no output voltage. This property of Wheatstone Bridge allows electrical cancellation of unwanted outputs, such as those resulting from temperature changes.

The output voltage from wheatstone bridge is given by the following expression (26) .

$$e = \frac{n}{4} K \epsilon_v G_f \quad \ldots \quad \ldots \quad \ldots \quad (2.1)$$

where,

a = Number of active arms in the bridge

$E_v$ = Input voltage to the bridge

$G_f$ = Gauge factor of the gauge

$\epsilon$ = Longitudinal strain in the gauge

Input voltage may be increased to increase the sensitivity of the bridge but heat dissipation capacity of the gauge is the limiting factor in this respect.

2.6 Strain Rings:

Strain rings provide a high ratio of sensitivity to stiffness. The fact that the inside surface of the ring is in an opposite state of strain from the outside allows four active arms to be efficiently used in a bridge circuit. The symmetry of a ring provides two parallel paths for heat flow which eliminate drift due to temperature gradient in the vicinity of the dynamometer.

Elastic investigation of circular ring shows that points 5,6,7 and 8 (Fig. 2.1) are the strain nodes for normal force $F_n$ and points 1,2,3 and 4 are the strain nodes for tangential force $F_t$. Also when both components of force are applied, points 1,3,5 and 7 are in tension and others are in compression. Thus by connecting gauges into two independent bridge both components of force can be measured simultaneously with minimum cross sensitivity.

For increasing rigidity we will use extended octagonal ring instead of a circular one (Figs. 2.2 and 2.3). The gauges will be placed at 45° from vertical axis instead of 39.6°, the theoretical angle. This simplifies

the mounting problem without appreciably affecting the performance. Further if the gauges are symmetrically placed this results in small cross-sensitivity.

2.6 Design Equations

2.6.1 Minimum Ring Thickness

In designing dynamometer, a compromise must be made between the sensitivity and the rigidity. This is controlled mainly by minimum ring thickness, which is calculated by using following formulae, derived from elastic ring theory (28).

$$t_r^2 = \frac{1.1\, F_n\, R_i}{E\, b_r\, \epsilon_t} \qquad \ldots \qquad \ldots \qquad \ldots \qquad (2.2)$$

where,

$t_r$ = Minimum thickness of octagonal ring, inch

$F_n$ = Normal force, lbs.

$E$ = Young's modulus of ring material, psi.

$\epsilon_t$ = Tensile strain in strain gauges 1 or 3, in/in

$b_r$ = Width of octagonal ring, inch

$R_i$ = Radius of the inside surface of ring, inch

2.6.2 Natural Frequency of the Ring

For the purpose of analysis any dynamometer can be reduced to a spring supported mass. The natural frequency of such a system is given by,

$$f_n = \frac{1}{2\pi}\sqrt{\frac{S}{M}} \qquad \ldots \qquad \ldots \qquad \ldots \qquad (2.3)$$

where,

$f_n$ = Natural frequency of ring cps.

S = Spring constant of the ring lb/in.

h = mass of the ring, lb $(sec)^2$/inch

In term of the weight of the ring 'W' equation (2.3) reduces to,

$$f_n = \frac{1}{2\pi}\sqrt{\frac{386\ S}{W}} \quad \ldots \quad \ldots \quad \ldots \quad (2.4)$$

Spring constant of ring is given by following relation (28):

$$S = \frac{1.39\ E\ b_r\ t_r^3}{R_1^3} \quad lb/in \quad \ldots \quad \ldots \quad (2.5)$$

2.7 Design Calculations:

2.7.1 Material Selection

Requirements of dynamometer ring material are:

a. good mechanical properties

b. good machinability

c. high heat conductivity

d. light in weight

e. corrosion resistance

In the present case Alumminum was used as the ring material.

2.7.2 Maximum Strain in the Gauges

The strain gauges cemented on the dynamometer had a gauge factor ($G_f$ = 2.82) of 2.82. These were manufactured by Rohits & Company (India) Roorkee.

Four channel recorder manufactured by Encardio Rite (India), Lucknow, was used for recording the forces during grinding. The maximum sensitivity available on this recorder was 0.0001 volts per cm of deflection.

For four arms active wheatstone bridge with input voltage of 12 volts equation (2.1) yields,

$$\epsilon/cm = 0.2955 \times 10^{-5} \text{ in/in} \quad \ldots \quad \ldots \quad (2.6)$$

It was observed that a normal force of 2 lbs gave 1 cm deflection on the recorder. Therefore, equation (2.6) gave,

$$\epsilon/lb = 1.4775 \times 10^{-6} \text{ in/in per lb of force}$$

Designing the dynamometer to measure maximum normal force of 225 lb, we have

$$\epsilon_{max} = 332.5 \times 10^{-6} \text{ in/in} \quad \ldots \quad \ldots \quad (2.7)$$

Dynamometers are subjected to repeated loading and unloading, therefore at higher strain values the fatigue life of the gauges are considerably reduced. It has been found that a strain gauge have an infinite life when operated at strains below $1000 \times 10^{-6}$ in/in (28). In the present case maximum strain was much lower than this value.

2.7.3 Maximum Stress Induced in Ring

At any instant strain in the ring and the gauges will be the same. The maximum stress ($\sigma_{max}$) induced in the ring when the maximum normal force is applied is given by

$$\sigma_{max} = \epsilon_{max} \times E = 3325 \text{ psi}. \quad (E \text{ for Al} = 10^7 \text{ psi}).$$

Yield point stress for Aluminum is 31800 psi which is much higher than the maximum stress induced in the ring. Hence ring will not undergo plastic deformation.

2.7.4 Minimum Ring Thickness

For four active arm bridge $0.2955 \times 10^{-5}$ in/in strain gives an output of 1 mm on the recorder. If only one arm is active then same output would be obtained by $4 \times 0.2955 \times 10^{-5}$ in/in strain which is equivalent to

$$\frac{4 \times 0.2955 \times 10^{-5}}{2.82} = 4.18 \times 10^{-6} \text{ strain / mm}$$

(where 2.82 denotes the gauge factor)

Assuming inside radius of the ring $R_i$ to be 1 inch and width of ring equal to $8 R_i$ and substituting $\epsilon_t = 4.18 \times 10^{-6}$ strain/mm in equation (2.2) we get

$$t = 4.02 \text{ mm}$$

We adopted 4 mm ring thickness. This reduction in ring thickness will increase the sensitivity of the dynamometer with a slight reduction in its stiffness.

2.7.5 Natural Frequency of Ring

The weight of ring was estimated to be 0.66 lb. Equations (2.4) and (2.5) yield

$$f_n = 334 \text{ cps.}$$

Spindle speed of grinding machine was 2700 rpm which gave an excitation frequency of 45 cps.

Thus the calculated frequency of dynamometer ring was more than 0.25 times the exciting frequency which signifies that the recorded force will not be influenced by vibrating motion during grinding.

2.8 Dynamic Response of the Dynamometer:

The octagonal ring was assembled with other components as shown in Fig.(2.5). Due to the various attachments the dynamometer ring was no longer rigid and its natural frequency will be considerably reduced. The exact value was obtained experimentally.

A wave form generator was used to generate sine wave and the output was fed to a power amplifier. The signal from the power amplifier excites electromagnetic vibration generator which induced vibrations in the dynamometer. The output from the dynamometer was fed to an oscilloscope.

Now the frequency of vibration was gradually increased till the natural frequency of the dynamometer was reached. At this frequency the amplitude increased significantly indicating resonance condition. This frequency was 279 cps; which was about 5 times more than the cutting frequency.

2.9 Calibration of the Dynamometer:

Both channels of the dynamometer were calibrated using dead weights and a pulley system as shown in Fig. (2.6). By plotting the calibration curve, it was found that the dynamometer had linear calibration. Some cross-sensitivity was also observed between the two channels.

Method of least square was used to find the equation of line of best fit through the experimental points. This is summarized below:

$$R_n = K_{nn} F_n + K_{nt} F_t \quad \ldots \quad (2.8)$$

$$R_t = K_{tn} F_n + K_{tt} F_t \quad \ldots \quad (2.9)$$

where,

$R_n$ = Total deflection on the normal force channel

$R_t$ = Total deflection on the tangential force channel

$F_n$ = Normal force

$F_t$ = Tangential force

$K_{nn}$, $K_{nt}$, $K_{tn}$ and $K_{tt}$ are constants of calibration curves.

From (2.8) we get,

$$\sum(\Delta R_n)^2 = \sum(R_n - K_{nn} F_n - K_{nt} F_t)^2 \quad \ldots \quad (2.10)$$

The necessary conditions for $\sum(\Delta R_n)^2$ to be minimum are,

$$\frac{\partial(\Delta R_n)^2}{K_{nn}} = \frac{\partial(\Delta R_n)^2}{K_{nt}} = 0 \quad \ldots \quad (2.11)$$

Equation (2.10) when operated with condition (2.11) yields,

$$K_{nn} = \frac{\sum R_n F_n}{\sum F_n^2} \quad \ldots \text{(for } F_t = 0\text{)} \quad \ldots \quad (2.12)$$

and

$$K_{nt} = \frac{\sum R_n F_t}{\sum F_t^2} \quad \ldots \text{(for } F_n = 0\text{)} \quad \ldots \quad (2.13)$$

Similarly constants of equation (2.9) were found to be,

$$K_{tn} = \frac{\sum R_t F_n}{\sum F_n^2} \quad \ldots \text{(for } F_t = 0\text{)} \quad \ldots \quad (2.14)$$

$$K_{tt} = \frac{\sum F_t \, F_t}{\sum F_t^2} \qquad \text{(for } t = n\text{)} \qquad \ldots \qquad (2.15)$$

From equations (2.12) to (2.15) we get the following calibration equations

$$R_n = 0.0197 \, F_n + 0.0134 \, F_t \qquad \ldots \qquad (2.16)$$

$$R_t = 1.1378 \, F_t + 0.1732 \, F_n \qquad \ldots \qquad (2.17)$$

A program was developed to find $F_n$ & $F_t$ from the recorded values of deflections $R_n$ and $R_t$.

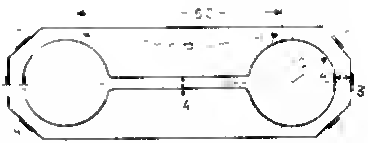

FIG 23 EXTENDED OCTAGONAL RING OF DYNAMOMETER

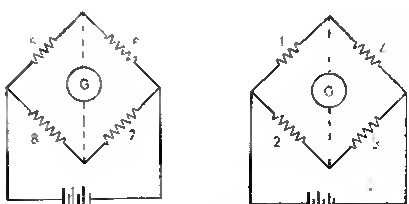

(a) (b)

FIG 24 WIRING DIAGRAM (a) HORIZONTAL FORCE CIRCUIT (b) VERTICAL FORCE CIRCUIT

FIG 2.5 DYNAMOMETER WITH THE BASE PLATE AND WORKPIECE

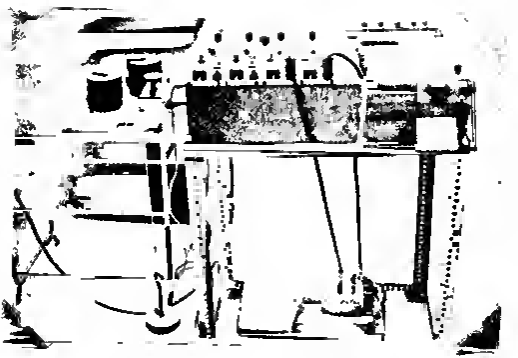

FIG 26 CALIBRATION OF THE DYNAMOMETER

## CHAPTER 3

## EXPERIMENTAL DETAILS

### 3.1 Grinding Machine:

A multipurpose precision horizontal surface grinding machine manufactured by Mirow Machine Tool Plant Vitebsk, U.S.S.R. was used under plunge cut conditions for the experiments. Some specifications of the machine are given below:

a. Table dimensions:(630 x 200) mm

b. Table longitudinal feed speed: maximum = 20 m/min

minimum = 3 m/min

c. Least count of vertical feed hand wheel scale: 0.001 mm

d. Maximum vertical stroke of grinding head: 375 mm

e. Grinding wheel details: (1) Dimension = (250 x 76 x 25) mm

(2) Spindle rpm = 2700

(3) Peripheral speed = 35 m/sec

Machine was equipped with standard electromagnetic plate.

### 3.2 Balancing of Grinding Wheels:

All grinding wheel used were balanced using four weights. Heavy spot was first determined (with the weights removed from the mount) and marked. Horizontal line 1-3 (Fig. 3.2) is drawn and weights were inserted

in the mount at 45° above and below the horizontal line. The two top weights were slightly moved upward to bring them closer. If out of balance still exsited the bottom weights were moved towards the horizontal line. Now position of new heavy spot was located, which was 90° away from its former position. With respect to the new position of heavy spot previous procedure was repeated until the wheel did not turn which indicated that the wheel was balanced.

3.3 Preliminary Experiment

Dynamometer was mounted on the magnetic base of the table and grinding machine was started. Warm-up time of 15 minutes was allowed before preliminary tests, which were carried out to ensure the following.

(a) Correct truing.

Ovai shape of the grinding wheel will appear as a thin circular ring, mounted on it, when the wheel is running. Absense of such appearance on wheel face ensures its concentricity with respect to its spindle and hence correct truing.

(b) Standardization of the dressing technique:

Different tools were used for truing and dressing. A new sharp pointed pyramid diamond was employed for dressing. The dressing diamond was mounted on a tool post with its natural cleavage point vertically upward and was made to touch the wheel at its bottom most point. Fine dressing under the following conditions gave repeatable results:

(i) Two passes at cross traverse of 1.2 mm/sec with depth of cut of 0.013 mm.

(ii) Two passes at cross traverse of 1.2 mm/sec with depth of cut of 0.005 mm

(3) Spark out.

Here one pass means front to rear and rear to front motion of dressing tool at a given depth of cut at the beginning of the forward motion.

(c) Proper functioning of the experimental setup:

The grinding dynamometer (discussed in chapter 2) was specially designed and fabricated for the purpose. Reliability trials of the dynamometer were performed to test the response and proper functioning of the dynamometer and the durability and consistency of its gauge circuits under continuous grinding. Proper working of the recorder and hydraulic drive of the grinding machine was also verified.

(d) Number of passes required to equilize the downfeed and the cut:

At the start of the grinding the depth of metal removed will be a fraction of downfeed due to the elasticity of the system. If the wheel is fed downward successively during each upstroke the depth of cut will quickly approach the downfeed. Number of such strokes required was found to vary between 15 and 20. After this equilibrium condition are reached the forces were recorded.

(e) Methods of establishing the beginning of re-dressing point:

The following phenomenon were observed when grinding reaches re-dressing point:

(1) Displacement of recording pen suddenly increased showing sharp increase in grinding forces.

(2) Workpiece surface had changed to grade temper colours resulting in

workpiece burn. This was due to high grinding temperature in the region of re-dressing point.

(3) Poor surface finish was visible.

(4) Metallic appearance appeared on the wheel face indicating increased loading on wheel.

(5) Side flow of the material along the edges of the workpiece was observed indicating ploughing and very little cutting.

(6) Increase in vibration was observed.

3.4 Grinding Conditions:

(a) Workpiece: The dimensions of workpiece are shown in Fig. (3.3). It was made out of rolled (50 x 16) mm mild steel flat.

(b) Grinding Wheels: Grinding wheels of three different hardness and grain sizes were used. These wheels were supplied by Carborundum Universal Ltd., Madras (India). Their details are given below:

1. A 36 - J8 - V 10
2. A 46 - J5 - V 10
3. A 46 - J8 - V 10
4. A 46 - L8 - V 10
5. A 60 - J8 - V 10

(c) Table Speed: 6 m/min, 10 m/min and 15 m/min

(d) Depth of Cut: 0.005 mm, 0.010 mm and 0.015 mm

(e) Wheel Speed: Kept constant at 35 m/sec

(f) Dry Grinding

(g) Fine Dressing

3.5 Sequence of Experiment

The dynamometer was mounted on magnetic base of the grinder and workpiece was brought in the centre of the wheel. The table speed was set at the required value and then wheel was started. Fifteen minutes warm-up time was allowed for the complete setup. Finally depth of cut was given during each up-stroke and forces were recorded. A representative force record during experiment is shown in Fig. (3.4). After some time (about 100 up-strokes) machine was stopped and reduction in wheel diameter was measured by dial gauge (least count 0.001 mm). Reduction in workpiece height was also measured with the accuracy of 0.02 mm. Tests were continued until the redressing condition was reached.

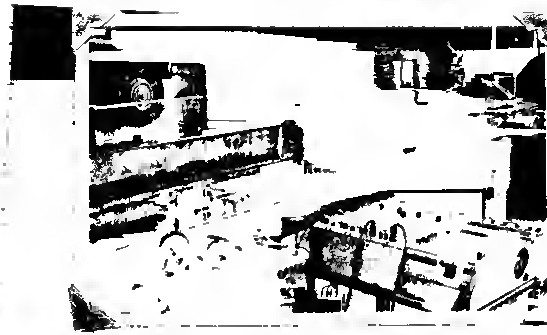

FIG 3.1 SET-UP OF THE EXPERIMENT

FIG 3.2 BALANCING STAND

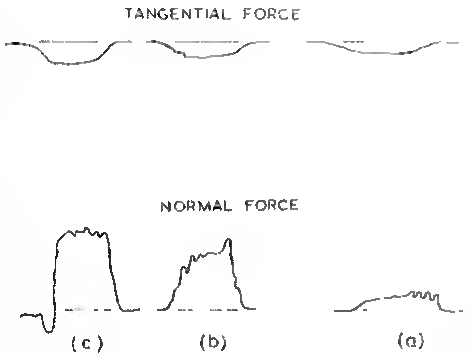


FIG 3 4 REPRESENTATIVE FORCE RECORD

(a) At V5 (wheel-life)

(b) At wheel-life

(c) Just after wheel-life

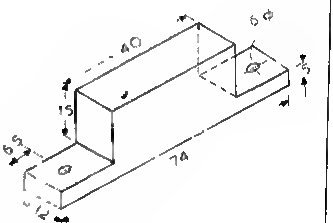


FIG 3 3 WORKPIECE DETAILS

(All dimensions in mm)

## CHAPTER 4

## RESULTS AND DISCUSSION

### 4.1 Force Traces:

Typical traces of tangential and normal forces are shown in Fig. 3.4. It is seen from the traces that the normal force shows more fluctuation than the tangential force. However, variation in the peak value of the normal force is small until about 1/3 of wheel life is reached as shown in Fig. 3.4(a). It appears from these traces that the deformation of the workpiece due to grinding heat is responsible for the variation in normal forces. Thermal deformation of the workpiece increases as the wheel approaches redressing point, producing increased variation in normal force as grinding proceeds. Normal force trace (Fig. 3.4(c)) just after the wheel life is reached shows that thermal deformation of the workpiece is so high that stable metal removal process is not possible. The tangential force traces, however, show negligible variation irrespective of grinding time.

### 4.2 Force Pattern During Grinding:

Using the recorded values of deflection, normal and tangential forces during grinding were calculated from the calibration equations 2.15 and 2.17. For various grinding conditions, variation of normal and tangential force with number of up-stroke were plotted as shown in Figs. 4.1 to 4.11.

These curves are similar to those obtained by previous workers (40, 46). It is seen from the plots (4.11, 4.6, 4.8, 4.9 and 4.10) that for the same material removal rate higher forces are obtained for the harder wheel (same grain size) or wheel with bigger grain size (same hardness). These results are similar to those previously reported (33, 43).

Typical force patterns (4.1) may be divided into three regions in the same manner as the wear curve discussed earlier:

(1) An unstable region where the forces rise to a peak and then fall to a steady value when finite wear flat is developed on sharp grains.

(2) A region of stable grinding condition where forces are constant and heat is in equilibrium. It seems that in this region the effect of truing to spark out has worn off and truely round wheel is obtained However, this region was only obtained at low material removal rate (Fig. 4.1).

A region of progressive built up of forces follows the region of stable grinding condition, where attritimne wear is predominant. Length of this region depends upon the reaction of the wheel to the particular combination of table speed and depth of cut.

(3) A region of sharp increase in forces where dulling of grains reaches a critical value and overheating develops, showing workpiece burn. Grinding becomes inefficient and redressing is required to regain the cutting ability of the grains.

Also Fig. (4.10) and Fig. (4.11) exhibit a constant force during grinding indicating the possibility that wheels A46-H5-V10 and A60-J5-V10

were soft for mild steel work material and give predominant fracture wear in region II.

4.3 Tool life of Grinding Wheel:

From the normal and tangential force patterns, end of phase II was independently located for both components of grinding force. The case of these two values was taken as the point where phase III begins. This defines the tool life of grinding wheel in terms of the number of up-strokes (N*), which is converted into seconds by using the following formula -

$$T^* = \left(\frac{0.06\ l_w}{v}\right) N^* \qquad \ldots \qquad \ldots \qquad (4.1)$$

where,

$T^*$ = Tool life of grinding wheel, seconds

$l_w$ = Length of workpiece, mm

$v$ = Table speed . . . . , m/min

Rate of material removal is estimated by using following formula -

$$V_R = \frac{v\ b_w\ d}{d0} \qquad \ldots \qquad \ldots \qquad \ldots \qquad (4.2)$$

where,

$V_R$ = Rate of material removal , $mm^3/sec$

$b_w$ = Width of workpiece , mm

$d$ = Depth of cut , micron

Table (4.1) shows the wheel life and the material removal rate for some sets of cutting conditions.

Table (4.1)

| Wheel | Cutting Conditions | | Tool Life of Grinding Wheel | | Rate of Material Removal |
|---|---|---|---|---|---|
| | V, m/min | d, micron | No. of up-strokes (Nw) | Seconds (Tw) | |
| A 36-J5-V10 | 10 | 5 | 282 | 68.5 | 4.02 |
| A 46-J5-V10 | 5 | 5 | 1020 | 490.0 | 2.0 |
| " | 5 | 10 | 220 | 100.5 | 4.0 |
| " | 5 | 15 | 91 | 41.5 | 6.0 |
| " | 10 | 5 | 564 | 151.5 | 4.0 |
| " | 10 | 10 | 171 | 39.0 | 8.0 |
| " | 10 | 15 | 92 | 31.0 | 12.0 |
| " | 15 | 5 | 578 | 91.6 | 6.1 |
| A 46-L5-V10 | 10 | 5 | 200 | 46.0 | 3.34 |

4.4 Grinding Ratio:

Force patterns for wheels A 46-M5-V15 and A 60-J5-V10 do not show the presence of region III, which indicates that force consideration for defining tool life is not valid under some cutting conditions. In order to evaluate grinding performance under conditions of varying hardness and varying grain size, economic aspect of various cutting conditions in terms of grinding ratio was investigated.

Volume of wheel wear is calculated by using following relation:

$$V_w = \frac{\pi}{2} D_g \cdot \delta(D_g) \cdot b_w \quad \ldots \quad \ldots \quad (4.3)$$

where,

$V_w$ = Volume of wheel wear , $mm^3$

$D_g$ = Wheel diameter , mm

$\delta(D_g)$ = Reduction in wheel diameter , mm

$b_w$ = Width of workpiece , mm

Wear curves showing the variation of volumetric wheel wear and volume of material removed were plotted. These are shown in Fig. 4.14, and are similar to those obtained by previous workers (37, 45, 46). The slope of the linear portion of these wear curves (region II) gives (Grinding Ratio).

Table (4.2) shows volume of material removed, volumetric wheel wear and grinding ratio for various wheels at a constant rate of material removal.

Table (4.2)

| Wheel | Grinding Ratio |
|---|---|
| A 46-H5-V10 | 5.2 |
| A 46-J5-V10 | 56.4 |
| A 46-L5-V10 | 20.0 |
| A 36-J5-V10 | 20.0 |
| A 60-J5-V10 | 10.2 |

4.5 Graphical Representation of the Results

A 46-J5-V10 wheel is extensively used for grinding mild steel, which was used in the present investigation also. This wheel was used

under different cutting conditions for establishing the tool life equation of the grinding wheel.

Variation of tool life with material removal rate is shown in Fig. (4.18) which shows that the tool life of grinding wheel decreases with increasing metal removal rate. On log-log plot this appears to be linear (Fig. 4.18). From our limited experimental data some preliminary conclusions can be drawn. As the table speed was increased the slope of the line decreased and these lines appear to intersect at almost same point on the tool life axis. This fact, however, should be verified from data for various table speeds. However, this appears to be reasonable from the consideration of forces acting on an individual grain . The linear plot of Fig.(4.18) based on these limited results appears to be related to the material removal rate by the following equation.

$$T^* (V_R)^n = C \quad \ldots \quad \ldots \quad \ldots \quad (4.4)$$

where,

$T^*$ = Tool life of grinding wheel, $V_R$ = Material removal rate

$n$ = Dynamic constant which depends on the table speed

$v$ = Table speed

$C$ = Static constant, which depends on the grinding wheel selected with the consideration of optimum grinding performance for the given material.

4.7 Linear Regression Analysis of the Results

4.7.1 Determination of Tool Life Equation:

Method of least square was used to obtain the line of best fit between the variables log $T^*$ and log $V_R$.

Equation (4.4) can be written as

$$\log T^* = \log C - n \log (V_R) \quad \ldots \quad \ldots \quad (4.5)$$

Assuming that the equation (4.5) represents line of best fit through the experimental points $(\log V_{R_1}, \log T_1^*)$, $(\log V_{R_2}, \log T_2^*)$ ... $(\log V_{R_n}, \log T_n^*)$, the sum of the square of the distance of experimental point from line (4.5) is given by,

$$q = \sum_{i=1} \left[\log T_i^* - \log C + n \log (V_{R_i})\right]^2 \quad (4.6)$$

Elimination of $\log C$ from equation (4.6) using equation (4.5) yields,

$$q = \sum_{i=1} \left[(\log T_i^* - \log T^*) + n (\log V_{R_i} - \log V_R)\right]^2 \quad (4.7)$$

$q$ can be seen to depend on $n$, and $n$ is chosen such that $q$ is minimum. The necessary condition for this is,

$$\frac{dq}{dn} = 0 \quad \ldots \quad \ldots \quad \ldots \quad (4.8)$$

Equation (4.8) when operated with condition (4.7) yields

$$n = -\frac{\sum_i (\log T_i^* - \log T^*)\ (\log V_{R_i} - \log V_R)}{\sum_i (\log V_{R_i} - \log V_R)^2} \quad (4.9)$$

In the above equation $\log T^*$ and $\log V_R$ represents mean value of two variables satisfying the line of best fit in equation (4.5). The value of dynamic constant calculated from equation (4.9) can be used in equation (4.5) for calculating the static constant.

Table (4.3) shows calculated values of two constant for two table speeds:-

Table (4.3)

| V, m/min | Dynamic constant 'n' | Static constant C |
|---|---|---|
| 5 | 2.361 | 2392 |
| 10 | 1.972 | 2392 |

4.6.2 Nature of dynamic constant

The general form of tool life equation for A 48-J5-W10 wheel is,

$$T^* (V_2)^n = 2392 \quad \ldots \quad \ldots \quad (4.10)$$

Using the experimental values for $T^*$ and $V_2$ ($T^* = 94.6$ sec ; $V_2 = 5.1$ m$^3$/sec) at table speed of 15 m/min, equation (4.8) yields

$$n = 1.782$$

It is seen from these results that dynamic constant decreases with increase in table speed. On log - log plot Fig. (4.18) variation of dynamic constant with table speed appears to be linear, which reveals that the dynamic constant must be related to the table speed by the following equation.

$$\log n + m \log v = \log C_1 \quad \ldots \quad \ldots \quad (4.11)$$

or

$$n v^m = K \quad \ldots \quad \ldots \quad (4.12)$$

Assuming that equation (4.11) represents the line of best fit, its slope ' $-m$ ' is given by the following equation deduced from equation (4.8)

$$n = -\frac{\sum_{i} (\log n_i - \log n)(\log v_i - \log v)}{\sum (\log v_i - \log v)^2} \qquad (4.13)$$

From equations (4.11) and (4.13) n and K are found to be 0.268 and 3.684 respectively.

Thus equation (4.12) becomes,

$$n = (3.684)\ (v)^{-0.268} \quad \ldots \quad \ldots \qquad (4.14)$$

Substitution for n in equation (4.10), gives us the final equation for the grinding wheel life,

$$T^{n}\ (v_w)^{(3.684)}\ (v)^{-0.268} = 939^{n} \quad \ldots \qquad (4.15)$$

This equation is very similar to Taylor's tool life equation and can be used to express the tool life of grinding wheel.

Material removal rate in grinding is proportional to the product of table speed and depth of cut. However, tool life equation (4.15) shows that increase in depth of cut adversely affects the tool life. Therefore for the same material removal rate, table speed should be fixed as high as possible depending on surface finish requirements and then depth of cut should be adjusted accordingly. With the present work it is recommended that for increasing the material removal economically, the table speed should be increased and not the depth of cut.

4.7 Prediction of Theoretical Values of Tool Life:

Experimental values of tool life for A 46-J5-V10 wheel which were established from force patterns (Figs. 4.1, 4.2, 4.3, 4.5, 4.6, 4.7) were

compared with the theoretical values predicted by tool life equation (4.15). These are given in table (4.4)

Table (4.4)

| v m/min | $V_s$ mm$^3$/sec | T sec. Theoretical | T sec. Experimental |
|---|---|---|---|
| 5 | 9.0 | 192 | 460.0 |
| 5 | 4.0 | 115.2 | 100.6 |
| 5 | 6.0 | 40.6 | 44.5 |
| 10 | 4.0 | 158.6 | 151.5 |
| 10 | 6.0 | 37.6 | 39.0 |
| 10 | 12.0 | 17.4 | 21.0 |
| 15 | 6.1 | 96.6 | 94.6 |

The tool life equation (4.15) which was established from the experimental analysis, reproduces the tool life values with very little difference. This indicates that equation (4.15) can be used to predict accurately the tool life for A 46-J5-V10 wheel under different cutting conditions.

4.6 Selection of Grinding Wheel

Two important parameters in the selection of grinding wheel are grade (hardness) and grain size. Previous results (37) seem to suggest that there may be optimum values of grade and grain size of grinding wheel for a particular work material for economic machining. The tool life

equation (4.15) should be used only after a suitable wheel has been selected. In order to investigate the economic aspect of grinding with different wheels, grinding ratios were plotted (Figs. 4.16 and 4.17) against wheel hardness and grain size. Fig. (4.16) shows the variation of grinding ratio with wheel hardness. This indicates that as the wheel hardness is increased, grinding ratio increases and reaches an optimum value for J hardness, while further increase in wheel hardness lowers the grinding ratio. Similar variation in grinding ratio is observed when grain size is increased from 36 to 60 with the optimum value of grinding ratio occuring for 46 grain size (Fig. 4.17). These results agree with those obtained by previous workers (37, 62).

The wheel with hardness H being a soft wheel is likely to have more fracture wear in comparison with attritious wear. As the wheel hardness is increased, for the same grain size, the amount of fracture wear will decrease and attritious wear will increase. At some hardness the best compromise between attritious and fracture wear is likely to reach where an optimum grinding ratio will be obtained. This signifies good grinding conditions. As the hardness of the wheel is increased from J to L attritious wear increases significantly. Grinding force, being strongly dependent on the wear flat area, will also increase. This increases the probability of grain fracture. Thus harder wheel is likely to have high attritious wear and significant grain fracture along with decreased material removal rate. This is also seen in Fig. (4.13) which indicates that A 46-I6-V10 wheel

have higher wear than that of A 46-J5-V10 but lower than that of A 36-J5-V10.

The reverse phenomena is likely to occur when grain size is increased from 36 to 60 (Increasing grain size number means smaller grain diameter). This is shown in Fig.(4.17). For wheels with larger grains, say 36, large rubbing areas will be associated giving high attritious wear and consequently high grinding forces, which is likely to cause more grain fractures. For smaller grains (high grain size number), fracture wear is likely to dominate attritious wear. In between these two extreme phenomenon an optimum grinding ratio is likely to be obtained. It must be pointed out that the selection of grain size on a wheel is also based on the surface finish requirements. Higher grain size number gives better finish (38, 43).

Variation of volume of material removed for different wheel hardness and grain sizes as grinding proceeds are shown in Fig. (4.12). It is seen from the plot that the maximum material removal occurs for A 36-J5-V10 L wheel and minimum for A 36-H5-V10 wheel while curve for wheel with hardness lies between the two and have dropping characteristics as grinding proceeds. This is due to the fact that harder wheels have more loading with chips, thus reducing the volume of material removed. Similar curves for wheels with different grain sizes but same hardness are shown in Fig. (4.12). The figure indicates that 46 grain size wheel will remove maximum volume of material and 36 grain size wheel will give least material removal (due to wheel loading), while curve for 60 grain size wheel lies between the two and have dropping characteristics as grinding proceeds.

It appears from the above discussion that if the wheel grinds in the self sharpening or predominant loading range grinding ratio will be low. However, in between these two, an economic grinding condition exists where wheel grinds in a zone of mixed conditions - partly self sharpening and partly loading, giving optimum grinding ratio.

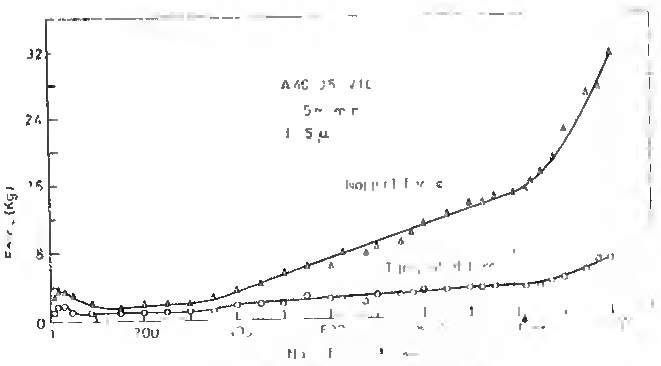


FIG 4.1 FORCE PATTERN DURING GRINDING

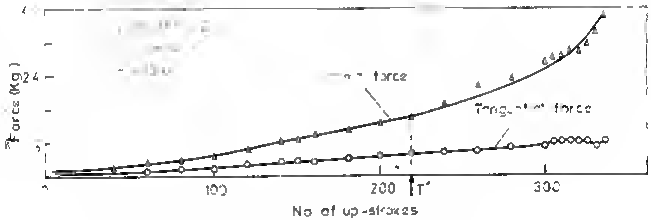


FIG 4.2 FORCE PATTERN DURING GRINDING

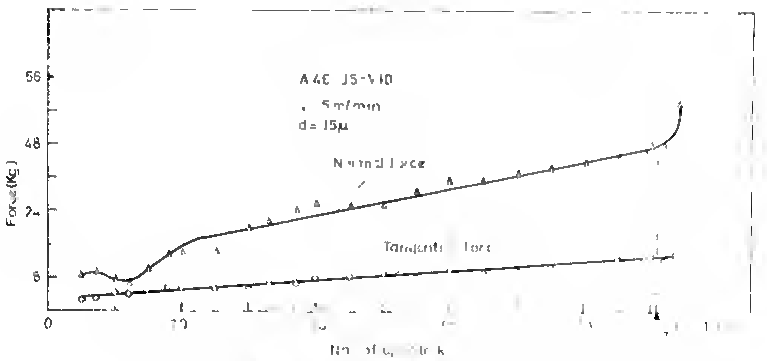


FIG 43 FORCE PATTERN DURING GRINDING

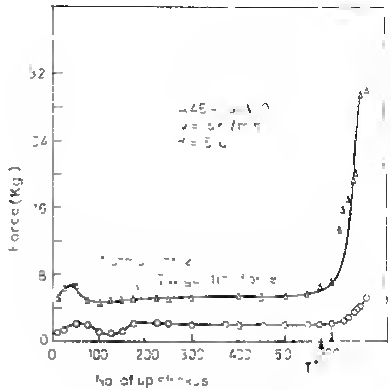


FIG 4.4 FORCE PATTERN DURING GRINDING

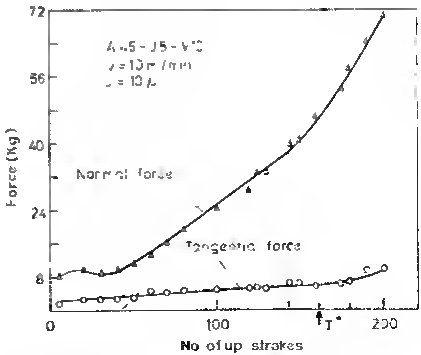


FIG 4.5 FORCE PATTERN DURING GRINDING

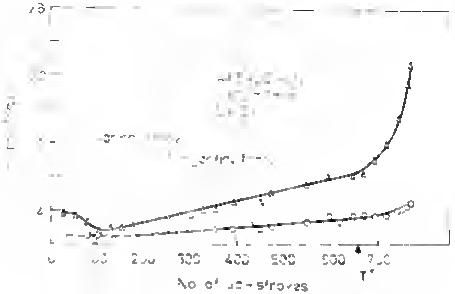


FIG 4.6 FORCE PATTERN DURING GRINDING

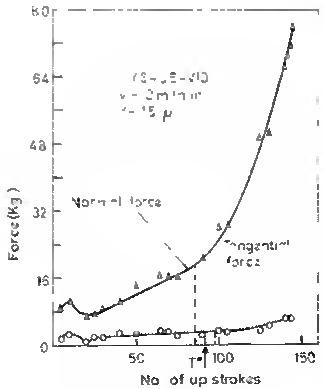


FIG 4.7 FORCE PATTERN DURING GRINDING

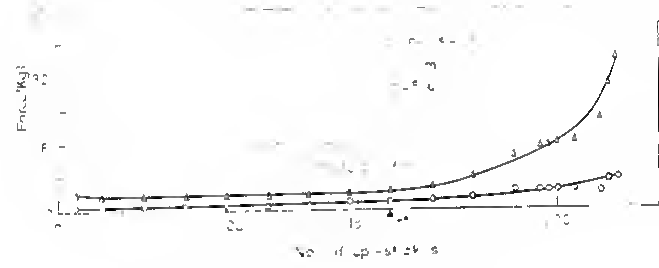

FIG 4.8 FORCE PATTERN DURING GRINDING

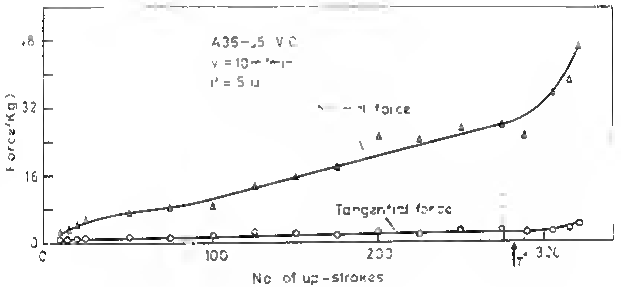


FIG 4 9 FORCE PATTERN DURING GRINDING

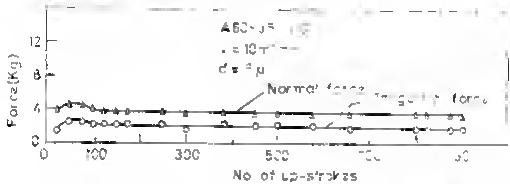


FIG 4-10 FORCE VARIATION DURING GRINDING

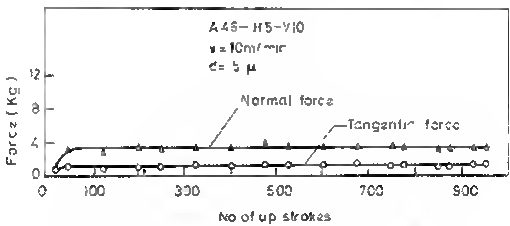


FIG 4 11 FORCE VARIATION DURING GRINDING

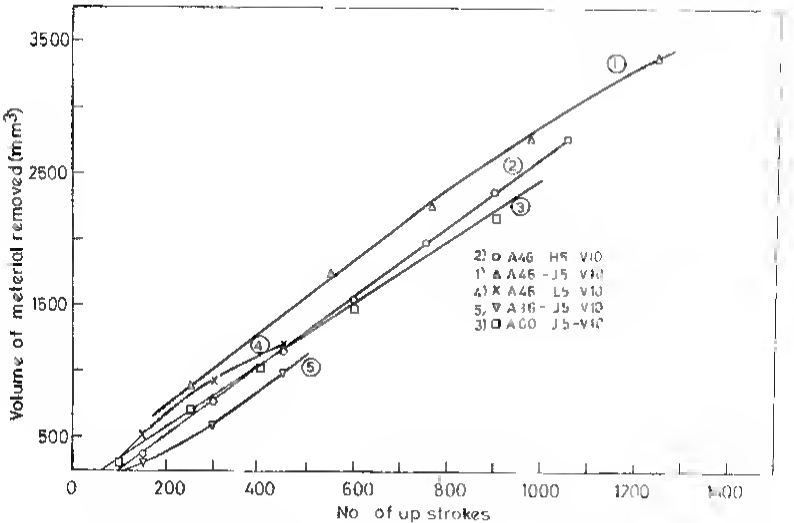


FIG 4.12 VARIATION OF VOLUME OF MATERIAL REMOVED WITH No OF UP-STROKES

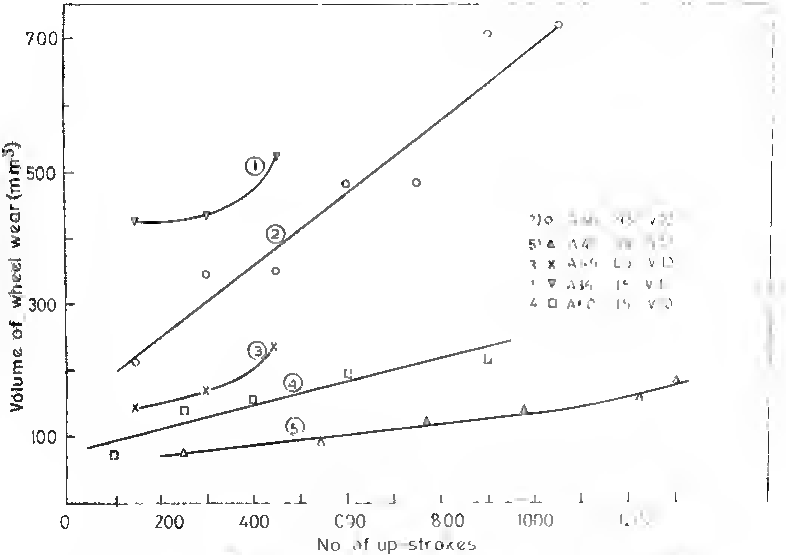


FIG 4.13 VARIATION OF WHEEL WEAR WITH No OF UP STROKES

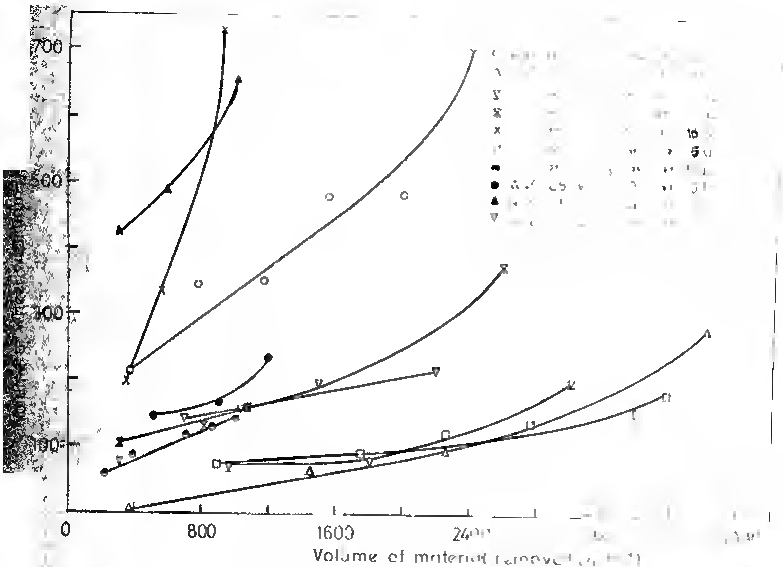


FIG. 4.14 VARIATION OF VOLUME OF MATERIAL REMOVED WITH TIME FOR WHEEL WEAR

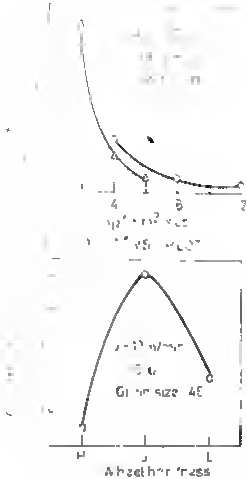


FIG. 4.11 VARIATION OF GRAIN HARDNESS

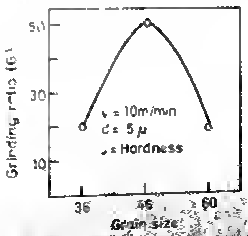


FIG. 4.12 VARIATION OF GRAIN SIZE

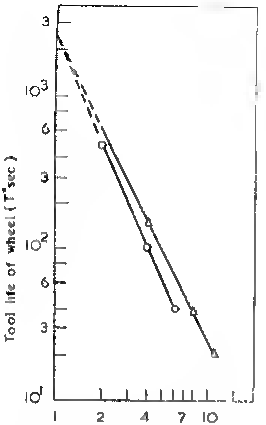


FIG 4.18 VARIATION OF $T^*$ WITH $V_R$ (Log-Log plot)

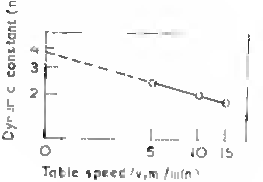


FIG. 4.19 VARIATION OF n WITH v (Log-Log plot)

5.3 Practical Importance of the Present Work

Present work may provide a guideline for locating the point during grinding when wheel requires dressing. Thus excessive wheel wear resulting due to uncertainty in wheel dressing may be reduced.

5.4 Scope for Further Work

By performing the tests during wet grinding under a wide variety of cutting conditions, the tool life equation established in the present work may be formulated into an ideal and practical form. Moreover wheel life may also be investigated with the considerations of wheel wear and surface finish.

## BIBLIOGRAPHY


1. W.W. Hutchinson, "Do we understand the Grinding Process", S.A.I. Journal, vol. 42, March 1930, p. 89.

2. H.M. Chapman, "Cylindrical Grinding in 1920", Trans. ASME, vol. 42, 1920, p. 596.

3. G.I. Alden, "Operation of Grinding wheels in Machine Grinding" Trans. ASME vol. 36, 1914, p. 401.

4. H.W. Wagner, "New Concepts of Abrasive Properties as affecting Grinding Performance", Mech. Engr., vol. 72, 1950, p. 223.

5. L.P. Tarasov, "Grinding Fundamentals I", Int. Prod. Res. Conf. Pgh. USA, 1963, p. 196.

6. N. Takenaka, "A study of Grinding action by single Grit", Annals of the CIRP, vol. 13, 1966, p. 183.

7. M.M. Friedman, S.M. Wu & P.T. Surathkar, "Determinations of Geometrical Properties of Coated Abrasive Cutting Edges", Trans. ASME, J. Engg. Ind., July 1973.

8. H. Opitz, K. Konig & C. Werner, "Kinematics and Mechanics in grinding with regard to the machining process", Proc. Int. Grinding Conf., Carnegie-Mellon University, Pittsburgh, U.S.A., April, 1972, p. 350.

9. M.C. Shaw, "The Grinding of Metals", Proc. Conf. on Tech. of Engg. Manufacture, I. Mech. E., London, 1958.

10. A.G. Vetten, "A Review of Theories of Metal Removal in Grinding", J. Mech. Engg. Science, vol. 11, No. 4, 1969.

11. C.K. Lal & M.C. Shaw, "On the dressability of Abrasive Grains", Int. J. MTDR, vol. 13, No. 3, Sept. 1973, p. 131.

25. P.S. Hahn, "On the nature of Grinding Process", Proc. 3rd Int, ach Tool Des. Res. Conf. Birmingham, Sept. 1962, p. 129.

26. T. Sasaki and K. Okamura, "The cutting mechanism of Abrasive grain", Bull. Japan Soc. of Mech. Engrs. vol. 3, 1960, p. 547,

27. N.H. Cook, E.G. Lowen & R.C. Shaw, "Machine Tool Dynamometer - s Current Appraisal", American Machinist, May 10, 1954, vol. 98, p. 125.

28. E.G. Lowen , E.E. Marshall & R.C. Shaw, "Electric Strain Gage Tool Dynamometer", Presented at the Society's Spring Meeting in Cleveland Ohio, May 27, 1950.

29. C.F. Yang, "Design of Surface Grinding Dynamometer", Trans. ASME, J. Engg. Ind., Feb. 1968, p. 197.

30. G.K. Lal & S. Stotar, "On the Wear of Grinding Wheels", Wear (In press).

31. G.K. Lal & M.C. Shaw,"Wear of single abrasive grain in fine grinding", Proc. 1st. Grinding Conf., Carnegie-Mellon Uni., Pittsburgh, USA, April 18-20, 1972, p. 107.

32. G.K. Lal, "Forces in Vertical Surface Grinding", Int. J. Mach. Tool Des. Res., vol. 8, 1968, p. 33.

33. S. Malkin & N.H. Cook, "The Wear of Grinding Wheels Part I Attritious Wear", Trans. ASME, J. Engg. Ind., vol. 93 B, Nov. 1971, p. 1120,

34. S. Malkin & N.H. Cook, "The Wear of Grinding Wheels Part 2 - Fracture Wear", Trans. ASME, J. Engg. Ind. vol. 93 B, Nov, 1971, p. 1123,

35. W.R. Backer & E.J. Krabacher, "New Techniques in Metal Cutting Research", Trans. ASME, vol. 78-B, 1956, p. 1497.

36. G.J. Goepfert & J.L. Williams, "The Wear of Abrasive in Grinding", Mech. Engg. vol. 81 - 1, 1959, p. 89.

37. E.J. Krabacher, "Factors Affecting the Wear of Grinding Wheels", Trans. ASME, J. Engg. Ind. vol. 81 b, Aug. 1959, p. 187.

38. F.J. Vickerstaff, "Wheel Wear and Surface Finish in Cross-feed Surface Grinding", Int. J. Mach. Tool Des. Res., vol. 13, No. 3, Sept. 1973, p. 183.

39. H. Ioshikawa & T. Sata, "Study on Wear of Grinding Wheels - 1 Bond Fracture in Grinding Wheels", Trans. ASME, J. Engg. Ind., vol. 85 B, 1963, p. 39.

40. P. Pollock, "The Wheel Wear & Metal Removal Mechanism in Vertical Spindle Machining of Steel", Trans. ASME, 1967.

41. R.P. Lindsay & R.S. Hahn, "On the Basic Relationship between Grinding Parameters", Annals of the C.I.R.P., 1971, p. 867.

42. J.K. Banerjee & K.J. Hillier, "Wheel Wear Pattern in Surface Grinding", Manufacturing Research, Feb. 1969, p. 59.

43. S. Kannappan & S. Malkin, "Effect of Grain Size and Operating Parameters on the Mechanics of Grinding", Trans. ASME, J. Engg. Ind, 1971.

44. H. Yoshikawa, "Fracture Wear of Grinding Wheels", Proc. Int. Conf. Prod. Engg. Sept. 1963, vol. 37, No. 4, p. 195.

45. B. Griebrook, "Precision Grinding Research", Production Engineer, May-June 196 , p. 38.

46. B. Grisbrook, R.H. Hollier & P.G. Varley, "Related Pattern of Grinding Forces, Wheel Wear and Surface Finish", Int. Prod. Res, vol. 1, No. 3, Aug. 1962, p. 37.

47. E.R. Marshall & M.C. Shaw, "Forces in Dry Surface Grinding", Trans. ASME, vol. 74, 1952, p. 51.

48. R.W. Storey, "Forces and Force Ratios in Grinding with Coated Abrasives", Trans. ASME, J. Engg. Ind. vol. 90 B, 1968, p 407.

49. J.K. Banerjee & K.J. Hillier, "Forces in Surface Grinding with Intermittent Cross-Feed", Manufacturing Research, Jan. 1969, p.63.

50. M.C. Shaw & D.A. Farmer, "An Analysis of Abrasive Machining of Plane Surfaces", Trans. ASME, J. Engg. Ind., 1965 p. 349

51. R.P. Lindsay, R.S. Hahn, "Variables Affecting Metal Removal and Specific Power in Precision Grinding", Annals of CIRP, vol. 21/1, 1971, p. 51.

52. G.B. Lor'c, "Evaluating the Performance of Grinding Wheels", Russian Engr. Journal 1967, p. 89.

53. H. Coldiss, "Applicability of the Grinding Equivalent", Annals CIRP vol. 20/1, 1971, p. 63.

54. H. Yoshikawa, "Theory of Tool Life for the Grinding Wheel", Annals CIRP, vol. 14, 1967, p. 343.

55. M.E. Zohdi & G. Smith, "Evaluating Tool Life of Semifinished Grinding", Mfg. Engg. & Management, vol. 65, No. 5, Dec. 1970, p. 22.

56. N.S. Zise, "Fracture of Abrasive Grain in Grinding", Trans. ASME J. Engg. Ind. vol. 88 B, Aug. 1967, p. 463.

57. R.P. Lindsay, "The Effect of Parameter Variations in Precision Grinding", Trans. ASME, J. Engg. Ind., vol. 92 B, Aug. 1970, p.883.

58. N. Nakayama, J. Brecker & M.C. Shaw, "Grinding Wheel Elasticity", Trans. ASME, J. Engg. Ind, Vol. 93 B, May 1971, p. 609.